Journal of Alloys and Compounds 983 (2024) 173921

Contents lists available at ScienceDirect

Journal of Alloys and Compounds

journal homepage: www.elsevier.com/locate/jalcom

Evidence of Gd substitution for Y in YBCO films with Gd excess

P. Reale [a], V. Pinto [b], P. Cayado [c,d], G. Celentano [b], A. Angrisani Armenio [b], A. Rufoloni [b], A. Santoni [a,*], F. D'Acapito [e]

[a] FSN-TECFIS-MNF, ENEA, v. E. Fermi 45, Frascati 00044, Italy
[b] Superconductivity Laboratory, FSN-COND, ENEA, Via Enrico Fermi 45, Frascati 00044, Italy
[c] Institute for Technical Physics, Karlsruhe Institute of Technology, Hermann-von-Helmholtz-Platz 1, Eggenstein-Leopoldshafen 76344, Germany
[d] Department of Quantum Matter Physics (DQMP), University of Geneva, Quai Ernest-Ansermet 24, Geneva 1211, Switzerland
[e] CNR-IOM-OGG, c/o ESRF, LISA CRG, c/o ESRF BP220, Grenoble F-38043, France

ARTICLE INFO

Keywords:
EXAFS
Superconductors
Atomic scale structure
Computer simulations
Chemical synthesis
YBCO
GdBCO

ABSTRACT

Gd-$YBa_2Cu_3O_{7-\delta}$ (Gd-YBCO) thin films with 10 mol% and 20 mol% excess-Gd concentration with respect to Y were investigated at the Gd L_3 and Y K core absorption edges by EXAFS spectroscopy with the aim of determining the local structure of the Gd dopant. To this purpose, EXAFS data were collected also on $GdBa_2Cu_3O_{7-\delta}$ (GdBCO) and pristine YBCO films and on Gd_2O_3 and Y_2O_3 model compounds for comparison with the YBCO films with Gd excess. The EXAFS analysis was based on Y and Gd oxides as well as on a cluster obtained by Density Functional Theory (DFT) where Gd atoms were inserted substitutional to Y atoms. The EXAFS data clearly reveal the incorporation of Gd in the lattice as substitute of Y and no evidence of segregated Gd oxide was found within the film matrix.

1. Introduction

High-temperature superconductivity has been a subject of intense research since the discovery of cuprate superconductors in the late 1980 s[1]. One of the most promising cuprate superconductors is the $YBa_2Cu_3O_{7-\delta}$ (YBCO) compound, which exhibits a high critical temperature (T_c) of around 90 K[2]. The YBCO compound in the form of thin films has important applications as for example in the development of superconducting cables for the production of the huge magnetic fields needed in the fusion reactor technology [3,4]. Even though YBCO tapes, or more generally Rare Earths – Barium - Copper Oxide (*RE*BCO) to which YBCO belongs, have already achieved performances suitable for applications, there is still room for further improvements, in particular of the critical current density (J_c) behavior in magnetic field conditions. Under these conditions, high J_c depends on the capability of preventing the movements of magnetic flux quanta, or vortices, created inside the superconductor, keeping them "pinned" by lattice or structural defects. The controlled introduction of suitable flux pinning centers for samples with excellent J_c behavior was successfully demonstrated [5,6]. Among others approaches, effective pinning centers in YBCO can be created by a doping with suitable nanodimensional oxide compounds[7] and by the addition of extra rare-earth (*RE*) elements to the YBCO lattice[8]. Following this scheme, Gd doping in YBCO in the substitutional (mixed) form of $RE_xY_{1-x}BCO$ [9–11] has been shown to improve the superconducting properties of YBCO thin films, including an increase in J_c because chemical substitution induces changes of the lattice properties in localized areas around the dopant which behave as defects that pin the vortices [12]. In case of Gd added in excess [13–15], improved critical current performances were reported, showing that effective pinning centers are promoted as well. On the other hand, in the latter case, an important question about the Gd fate in Gd-YBCO systems concerns the arrangement of the dopant in the lattice when Gd is added in excess with respect to Y ($Gd_xYBa_2Cu_3O_{7-\delta}$ Gd-YBCO): does the Gd dopant substitute Y in the lattice or does it agglomerate in different phases? Clearly, determining the atomic arrangement is an important step for understanding the physical-chemical properties of the mixed cuprate compounds. In the case of Gd-YBCO, it is reasonable to expect either the Gd substituting Y in the YBCO lattice with the subsequent formation of Y oxides such as Y_2O_3 or simply the direct formation of Gd oxides if no substitution occurs. This issue has been addressed in a previous work by Pinto *et al.* [15] where X-Ray Photoelectron Spectroscopy (XPS) and Scanning Transmission Electron Microscopy (STEM) results on excess 5% and 10% Gd-YBCO films grown by Chemical Solution Deposition (CSD) have shown that Gd was uniformly dispersed in

* Corresponding author.
E-mail address: antonino.santoni@enea.it (A. Santoni).

https://doi.org/10.1016/j.jallcom.2024.173921
Received 30 August 2023; Received in revised form 25 January 2024; Accepted 18 February 2024
Available online 20 February 2024

the YBCO matrix. The need to better clarify the fate of Gd in Gd-YBCO film it is not merely driven by academic curiosity but it is related to a more fundamental issue aimed at the assessment of the full potentiality of this approach for J_c improvements. In fact, a huge number of studies have been already carried out on the introduction of Artificial Pinning Centers (APCs) in *RE*BCO film by CSD [16–22]. However, the obtained $J_c(B)$ enhancement could still not compete with those of the analogous films made by physical methods, especially at low temperatures and high magnetic fields [5,23,24]. Therefore, a deeper comprehension of the growth process of mixed *RE*BCO materials could allow to better manage the introduction of nanometric defects obtained through CSD method.

In this work, an EXAFS investigation of the structure of excess Gd-YBCO films with 10% and 20% excess Gd (with respect to Y) is presented, with the aim to ascertain the behavior of Gd in the YBCO lattice and possibly confirm the results about the local structure reported in Ref. [15]. The data obtained from the Gd-YBCO films are compared with GdBCO and YBCO thin films, Y_2O_3 and Gd_2O_3 powders and with an ab-initio theoretical model of a YBCO relaxed lattice containing Gd in the first Y neighbor shell.

2. Materials and methods

2.1. Sample preparation

A low-fluorine Metal Organic Decomposition route was used for preparing highly-epitaxial standard YBCO and excess Gd-YBCO thin films with 10 mol% and 20 mol% excess-Gd concentration with respect to Y. The precursor solution was obtained dissolving in propionic acid Y, Gd, Ba and Cu metalorganic salts in the stoichiometric ratio of 1: *x*: 2: 3, where $x = 0$; 0.1; 0.2 for YBCO, Gd10%-YBCO, Gd20%-YBCO respectively. The films, about 80 nm thick, were deposited on $SrTiO_3$ (100) single crystals by spin coating. The crystallization step was carried out at a temperature equal to 830 °C in a humid mixture of nitrogen and oxygen (flow rate N_2: 2.83 L min^{-1}, O_2: $1.15{\cdot}10^{-3}$ L min^{-1}). A further treatment was performed at 450 °C in pure oxygen flow in order to promote the complete *RE*BCO oxygenation. More details on solution preparation and on the thermal treatment are provided in Refs. [15,25]. The GdBCO precursor solution was obtained dissolving in anhydrous methanol Gd, Ba and Cu metalorganic salts in the stoichiometric ratio of 1: 2: 3. Films were prepared by depositing the precursor solution on $LaAlO_3$ single crystals via spin coating. The crystallization step was carried out at the temperature of 810 °C with an oxygen content equal to 50 ppm. The film thickness was 220 nm. The preparation techniques are extensively reported in Refs. [10,26].

2.2. Film characterization

The morphology was investigated through Scanning Electron Microscopy (SEM) images recorded by a Gemini LEO 1525 field emission high-resolution SEM with 10–20 kV accelerating voltage and in-lens high-resolution annular detector. X-ray diffraction (XRD) analysis was performed to study the film structural properties. A Rigaku Geigerflex diffractometer with Cu Kα radiation was used in a Bragg Brentano configuration.

The zero-resistance critical temperature, T_c, was assessed through *R* (*T*) measurements performed by d.c. electric measurements in the four-probe configuration with a 2420 Keithley current sourcemeter (used current 100 μA) and a 2182 A Keithley nanovoltmeter. Oxford vibrating sample magnetometer (VSM) equipment provided with a superconducting magnet was used for the analysis of magnetic properties.

2.3. X-ray absorption spectroscopy

Extended X-ray Absorption Fine Structure (EXAFS) is measured at a core (typically K or L) absorption edge and is due to the interference of the absorber's photoelectron wave with the scattered waves from the neighbor atoms. By measuring and analyzing the oscillatory variations of the x-ray absorption signal as a function of energy, it is possible to achieve information about the environment around the absorber atom.

2.4. Data collection

EXAFS measurements were carried out at the Italian CRG beamline LISA [27] at the ESRF (Grenoble, France). Si(111) crystals were used for the monochromator and Si(Pt) coated collimating/focusing mirrors were used for the Gd-L_3 @ 7243 eV (Y-K @ 17038 eV) edges. Data were collected at room temperature and in fluorescence mode using a 12 elements High Purity Germanium detector. In order to enhance the signal from the thin film a grazing incidence geometry was adopted with the sample surface perpendicular to the beam polarization vector and an incidence angle of 5°. The Gd_2O_3 and Y_2O_3 model compounds were obtained from commercial powders and pressed in pellets using cellulose as binder and limiting the maximum absorbance to $\mu \leq 1.5$ in the spectrum energy range. The Gd_2O_3 and Y_2O_3 standards were measured in transmission mode.

2.5. Data analysis

EXAFS spectra were extracted with the ATHENA code and fitted with the DEMETER 0.9.26 package [28]. The theoretical EXAFS signals were calculated with the FEFF-6 code embedded in DEMETER. For the model compounds the structures Y_2O_3 [29], YBCO [30], Gd_2O_3 [31] and GdBCO [32]were considered for the generation of the theoretical EXAFS paths. The theoretical paths of Gd in YBCO were generated from a cluster obtained by Density Functional Theory (DFT) as implemented in the VASP [33] code. A unit cell of YBCO taken from the crystallographic determination was firstly relaxed and from that a 331 supercell was derived. In this supercell 2 Gd atoms were inserted substitutional to 2 Y (a central Y and a 4th neighbor) and the supercell was relaxed again. Calculations were done with projector augmented wave (PAW) pseudopotentials and the exchange-correlation functional used was the Perdew–Burke–Ernzerhof for solids (PBEsol) [34]. At each ionic step, the electronic structure has been optimized until attaining a convergence of the total energy within 10^{-6} eV, whereas the atomic positions were optimized until Hellman-Feynman forces were below 10^{-3} eVÅ^{-1}.

3. Results and discussion

3.1. Film properties

In Fig. 1 the SEM images of YBCO films deposited on STO with different Gd content are shown. YBCO films exhibit the typical morphology of MOD deposited samples showing a compact and flat surface with complete grain coalescence (Ref.[15]). The presence on the surface of randomly distributed spherical particulates, with size about 100 nm or smaller, can be also recognized. These particulates were often assigned to secondary phases, mainly binary oxides, such as (Y, Gd)$_2$Cu$_2$O$_5$, or Cu oxides segregated at the surface during the YBCO film growth stage (see Fig. S1 in the Supplementary Materials of ref.[15]). The introduction of 10% Gd in excess of Y appears quite ineffective to the film morphology. SEM images reveal very similar features of the pristine YBCO film (see Fig. 1b) with a slight increase in the presence of spherical particulates on the surface. On the other hand, a further increase in Gd introduction up to 20% in excess with respect to Y leads to a dramatic change in the film morphology characterized by the presence of a relevant fraction of *a*-axis grains with their typical needle behavior and as well as slightly tilted grains. Due to this, the surface appears more disordered with not complete coalescence among grains (Fig. 1c). It is worth noticing that the high content of *a*-axis grains (Fig. 1c) of the Gd20%-YBCO sample is probably due to the adopted thermal treatment that is optimized for YBCO growth, but not for GdBCO [35,36].

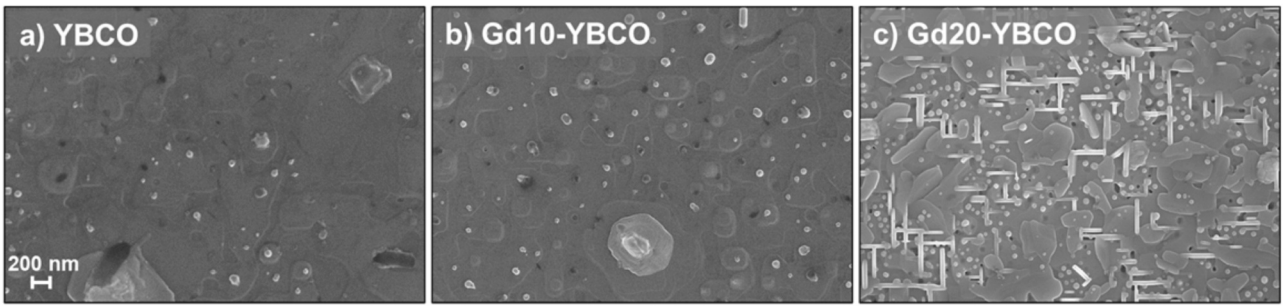

Fig. 1. SEM images at the same magnification of (a) YBCO, (b) Gd10-YBCO, and (c) Gd20-YBCO films. Scale bar: 200 nm.

Remarkably, there is also a large increase in the density of spherical particulates. TEM analysis carried out on 5%Gd-YBCO films [15], revealed a mixed composition Y-Gd-Cu (a reliable quantitative estimate has not been possible) in the spherical particulates consistent with the formation of a $(Y,Gd)_2Cu_2O_5$ phase. Assuming that a similar feature could be extended to films with higher excess of Gd, one can infer that increasing Gd content promotes the formation of $(Y,Gd)_2Cu_2O_5$ phases. In addition, no traces of Y_2O_3 crystals was detected by TEM [[15]]. More insight can be gained by analyzing the XRD spectra of these films. In Fig. 2, the relevant part of the spectrum for YBCO and Gd-YBCO samples are shown. The presence of the (004) YBCO peak reveals that all films are mainly *c*-axis oriented. However, the low angle shift of the peak position in Gd-YBCO films is consistent with a mixed YBCO+GdBCO reflection with a smaller fraction of GdBCO phase (e.g. PCPDF cards # 410173 and 381433 for GdBCO7 and YBCO7, respectively). This would imply that at least some fraction of the introduced Gd forms GdBCO phases, with Gd ions occupying the same crystallographic position of Y in YBCO. In addition, reflections related to the presence of binary oxides progressively increase with the Gd excess. In particular, peaks ascribable to $RE_2Cu_2O_5$ clearly emerged in the spectrum of 20% Gd. A similar behavior is shown by the reflection peaked at about 29.5° consistent with increasing contributions of RE_2BaO_4 or RE_2BaCuO_5 in the film with 20% Gd excess. Similarly to the (004) peak shift, the shift of this peak to lower angles is coherent with a reduced Y fraction in $(Gd,Y)_2BaO_4$ and $(Gd,Y)_2BaCuO_5$ systems. Interestingly, no clear peaks ascribable to RE_2O_3 can be detected in the spectra of YBCO and Gd-YBCO films. Another remarkable feature is the presence of a broad high angle tail of the (004)YBCO peak in the 20% Gd-YBCO film consistent with the increased contribution of $RE_2Cu_2O_5$, RE_2BaO_4 or RE_2BaCuO_5 secondary phases.

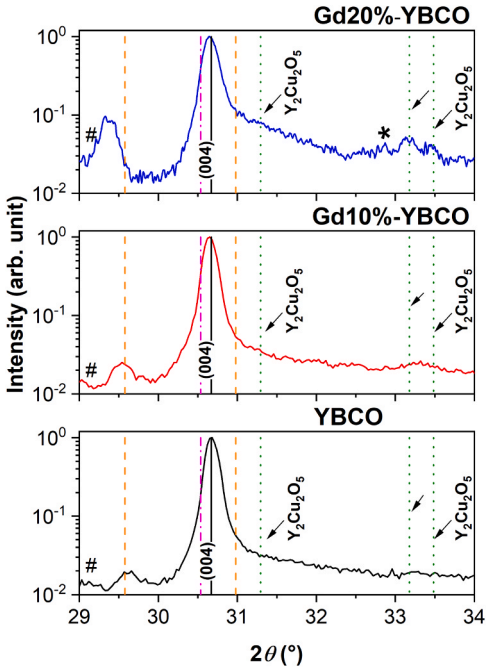

Fig. 2. X-ray θ−2θ patterns of different samples. The vertical lines indicate the peak position ascribed to (004)YBCO (continuous black line), (004)GdBCO (dash dotted magenta line), Y_2BaO_4 (dashed orange line), and $Y_2Cu_2O_5$ (dotted olive line). The symbols # and * indicate the Y_2O_3 and (103)YBCO peak positions.

The superconducting properties of YBCO and Gd-YBCO films were evaluated by measuring T_c and J_c values. First of all, a slight increase of the T_c values due to Gd addition can be recognized, namely 90.2± 0.4 K, 90.3± 0.1 K, and 90.8± 0.2 K, for YBCO, Gd10%-YBCO, Gd20%-YBCO, respectively. This result is consistent with the T_c of GdBCO generally higher than YBCO, i.e. around 94 K [36,37]. J_c data at most relevant conditions are summarized in Table 1. As it can be seen, at 77 K Gd20%-YBCO exhibited self-field J_c values comparable to pure YBCO ones but lower than Gd10%-YBCO. Apart from this, similar magnetic field dependences were recorded as shown by the data at 1 T and 3 T. The presence of a high content of *a*-axis grains in Gd20%-YBCO (Fig. 1c) can explain this behaviour at 77 K. On the other hand, at 10 K an evident increase in J_c dependence from magnetic field can be appreciated. When an external magnetic field is applied, Gd20%-YBCO films showed improved J_c values at both 1 and 3 T with respect to the undoped film. Moreover, when the J_c values are normalized with respect to the self field J_{c0}, the improvement of in-field Gd20%-YBCO performances is more evident (Fig. 3). Hence, the introduction of Gd in YBCO leads to a strengthened J_c behavior in magnetic field mainly at low temperatures. This indicates that Gd excess promotes vortex pinning introducing pinning centers effective at low temperatures.

3.2. Qualitative analysis

The EXAFS data will be discussed here in a qualitative way.

Fig. 4a shows the EXAFS signals ($k^2\chi(k)$) measured at the Gd L_3 edge of the reference compound GdBCO and superimposed to the $k^2\chi(k)$ of Gd20%-YBCO sample. The reference GdBCO and Gd20%-YBCO spectra appear nearly identical indicating that the environment around the Gd

Table 1
Critical current density (J_c) measured with VSM at 77 K and 10 K and different applied magnetic fields.

Temperature (K)	Applied Field (T)	YBCO[1] (MA·cm^{-2})	Gd10%-YBCO (MA·cm^{-2})	Gd20%-YBCO (MA·cm^{-2})
77	0	1.71 ± 0.64	2.75	1.30
	1	0.10±0.02	0.11	0.12
	3	0.02 ± 0.01	0.02	0.02
10	0	15.5±0.6	21.3	14.1
	1	3.29±0.65	4.53	4.15
	3	1.80±0.37	2.43	2.30

1the mean and standard deviation of results obtained for several samples prepared in the same laboratory and with the same procedure are provided.

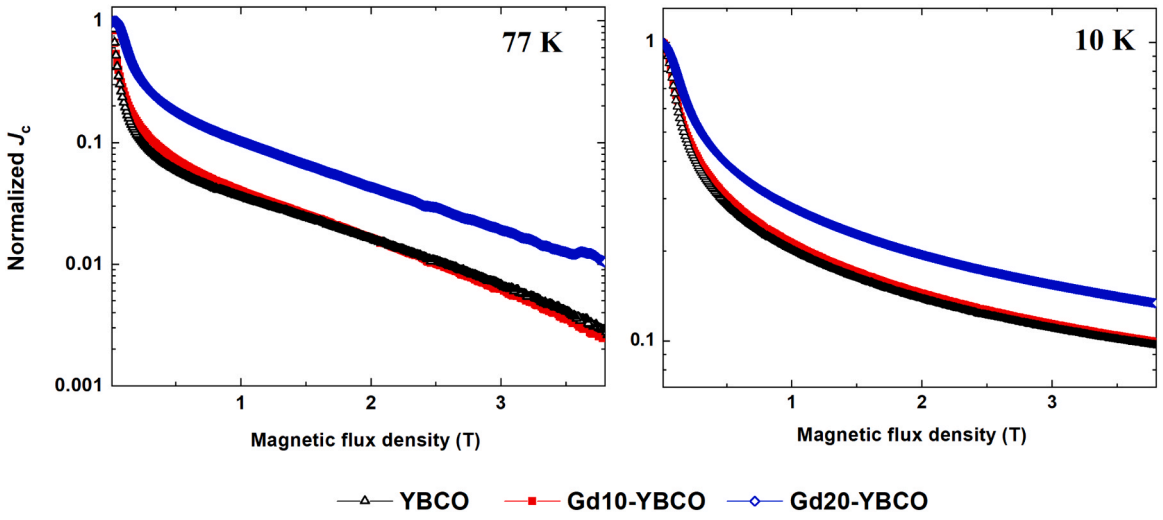

Fig. 3. Critical current density normalized with respect to the self field value as a function of the applied magnetic field recorded by VSM for pristine YBCO (black open triangle), Gd10%-YBCO (red full square) and Gd20%-YBCO (blue open diamond) films at 77 and 10 K with H//c-axis condition.

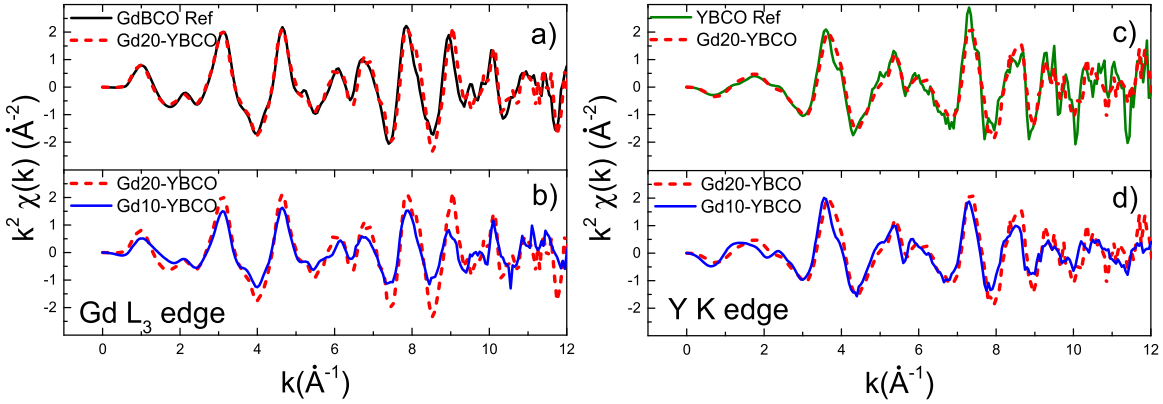

Fig. 4. a) GdL_3 edge, GdBCO reference (black continuous line) and Gd20% doped-YBCO (red dashed line) $k^2\chi(k)$ EXAFS signals; b) GdL_3 edge, Gd20% doped-YBCO (red dashed line) and Gd10% doped-YBCO (blue continuous line) $k^2\chi(k)$ EXAFS signals; c) Y K edge, YBCO reference (green continuous line) and Gd20% doped-YBCO (red dashed line) $k^2\chi(k)$ EXAFS signals; d) Y K edge, Gd20% doped-YBCO (red dashed line) and Gd10% doped-YBCO (blue continuous line) $k^2\chi(k)$ EXAFS signals.

absorber is similar. Fig. 4c shows the $k^2(k)$ data obtained at the Y K edge of the reference YBCO and the Gd20%-YBCO sample. The superimposed data are again similar up to about 10 Å^{-1}, showing in this case that the atomic environment around the Y absorber is not much affected by the Gd doping. However, small intensity differences are visible indicating the presence of disorder in the YBCO lattice around the Y absorber

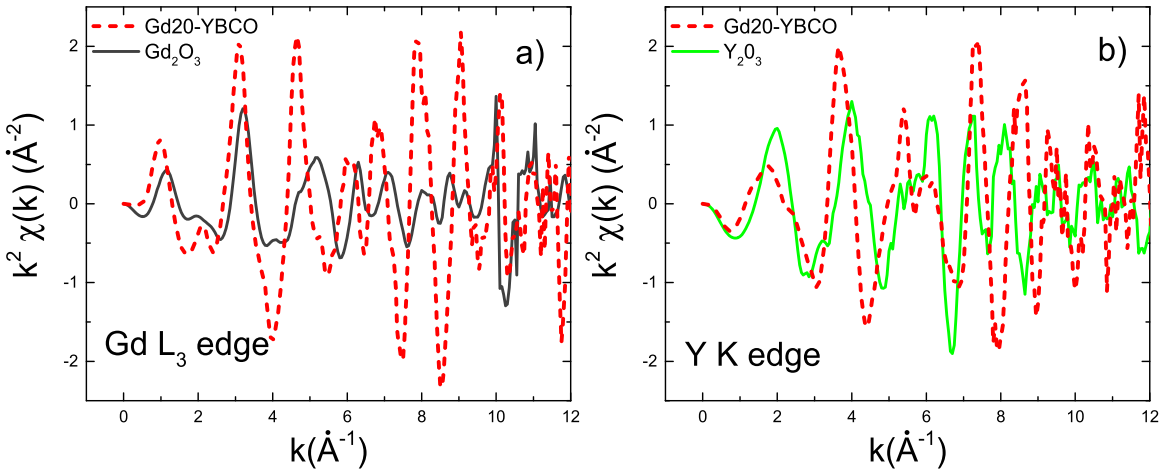

Fig. 5. a) GdL_3 edge: Gd_2O_3 reference (dark grey continuous line) and Gd20% doped-YBCO (red dashed line) $k^2\chi(k)$ EXAFS signals; b) Y K edge: Y_2O_3 reference (green continuous line) and Gd20% doped-YBCO (red dashed line) $k^2\chi(k)$ EXAFS signals.

probably because of the Gd addition. In Fig. 4b the Gd L_3 Gd10%-YBCO data show that the structure of the oscillations is similar to the Gd20%-YBCO although with a lower amplitude. At the Y-K edge (Fig. 4d) the Gd10%-YBCO amplitude is similar to the 20%-doped sample up to about 7 $Å^{-1}$ and becoming smaller at higher k. Lower amplitude oscillations are presumably due to an increased structural disorder. These two cases strongly suggest the occurrence of Gd in an environment close to that found in the reference GdBCO. The environment of Y is not dramatically altered by the presence of Gd further supporting the idea of incorporation of Gd in the YBCO lattice substituting for Y.

In Fig. 5a and b the Gd20-YBCO data are superimposed for comparison to the EXAFS signals of the Gd_2O_3 and Y_2O_3 at the Gd L_3 and Y K edge, respectively. Data show that the shape and intensity of the Gd and Y oxides are very different from the Gd-doped YBCO films ruling out the hypothesis of segregation of these ions in these oxide phases. In order to estimate a minimum detectable secondary phase, we have constructed spectra of mixed x*Gd_2O_3 + (1-x) GdBCO with x=2, 5, 10 and 20% and made a linear combination fitting with the original phases to determine the minimum detectable. Simulations of mixed-phase spectra revealed that the minimum detectable secondary phase is 5%.

3.3. Quantitative analysis

The quantitative analysis was carried out by calculating theoretical EXAFS paths with the FEFF6 code starting from the crystallographic structures of the model compounds or the cluster obtained by the DFT. As Fig. 6 suggests, the structural model consisted in a first (Absorber)-O shell (Fig. 6a), a second (Absorber)-Cu shell (Fig. 6b), a third (Absorber)-Ba (Fig. 6c) and a fourth (Absorber)-(Y/Gd) mixed shell (Fig. 6d) with Absorber = Y or Gd depending on the edge under analysis. The 4th shell was considered as composed by 4 atoms either Gd or Y with variable occupation implemented via the Y fraction parameter Y_{frac} (variable from 0 to 1). With a nominal Gd doping = 0.2, the expected Y_{frac} value is 0.8. The fitted Y_{frac} parameter resulted 0.6 ± 0.1. However, this value is considered to be acceptable accounting for the model complexity (5 shells are necessary to reproduce the data) and noise in the data. Table 2 summarizes the results of the EXAFS analysis, while the reference parameters for the YBCO and GdBCO lattices and for the DFT VASP model are summarized in Table 3.

Fig. 7a shows the magnitude of the Fourier transform (FFT) of the Gd20%-YBCO EXAFS signal taken at the Gd L_3 edge and the magnitude of the FFT of the fitted theoretical EXAFS spectrum. The fitting within the same scheme of the data for Gd10%-YBCO EXAFS at the Gd L_3 edge gives a similar result, which is shown in Fig. 7b.

The structural parameters of the DFT models (Table 3) are in good agreement with the experimental data (Table 2) further supporting the picture of the Gd excess atoms substituting Y in the YBCO lattice. Results indicating a possible substitution of Y with Gd in the Gd-doped YBCO lattice have been reported in recent work [15]. In that work XPS and High-Angle Annular Dark-Field STEM (HAADF-STEM) data showed the possible presence of Gd atoms in Y sites, in accord with the EXAFS results presented here. More, STEM microscopy detected stacking faults in the film bulk in form of broadly dispersed $YBa_2Cu_4O_8$ (Y124) intergrowths causing strain in the YBCO matrix. This kind of defects and lattice distortions may affect the EXAFS data and could be a possible explanation for the observed amplitude differences in the $k^2(k)$ of different samples and uncertainties in the fitting results.

In addition, it is worth noting that the signal of interest is generated by the fourth shell which is influenced by the interference of the heavy Ba atoms in the third shell and could play a role in the correct determination of the stoichiometry.

Table 2
Results of the EXAFS analysis at the Gd-L_3 edge for the Gd20%- and Gd10%-YBCO films.

		Gd20-YBCO		Gd10-YBCO	
shell	**N**	σ^2 ($Å^2$)	**R (Å)**	σ^2 ($Å^2$)	**R (Å)**
1st O	8(1)	0.005 (1)	2.42 (2)	0.006 (1)	2.42 (2)
2nd Cu	8(1)	0.004 (1)	3.22 (3)	0.007 (1)	3.24 (3)
3d Ba	2.0 (3)	0.002 (1)	3.69 (3)	0.005 (1)	3.71 (3)
4th Y	2.5(5)	0.003 (1)	3.85 (4)	0.006 (1)	3.84 (4)
4th Gd	1.6(5)	0.002 (1)	3.89 (4)	0.004 (1)	3.80 (4)

N is the coordination number. $\boldsymbol{\sigma}^2$ is the EXAFS Debye-Waller factor and R is the absorber-scatterer distance.

Table 3
Reference parameters for the YBCO and GdBCO lattices and for the DFT VASP model.

shell	R_{Y-x} (Å) YBCO[ref.18]	R_{Gd-x} (Å) GdBCO [ref.20]	R_{Gd-x} (Å) Gd:YBCO [VASP]
1st O	2.39	2.41	2.39
2nd Cu	3.21	3.22	3.19
3d Ba	3.69	3.68	3.65
4th Y	3.82–3.89		3.81
4th Gd		3.85–3.90	3.87

4. Conclusions

In summary, Gd-doped YBCO films with improved superconducting performances were studied by EXAFS with the aim of determining the position of the Gd atoms in the YBCO lattice. Results from the comparison of the $k^2\chi(k)$ EXAFS data with undoped standards and the fitting to a theoretical ab-initio DFT relaxed lattice model containing a Gd atom in the first-neighbour Y shell have indicated that the Gd atoms assume the positions of Y in the doped lattice. Possible other Gd-related

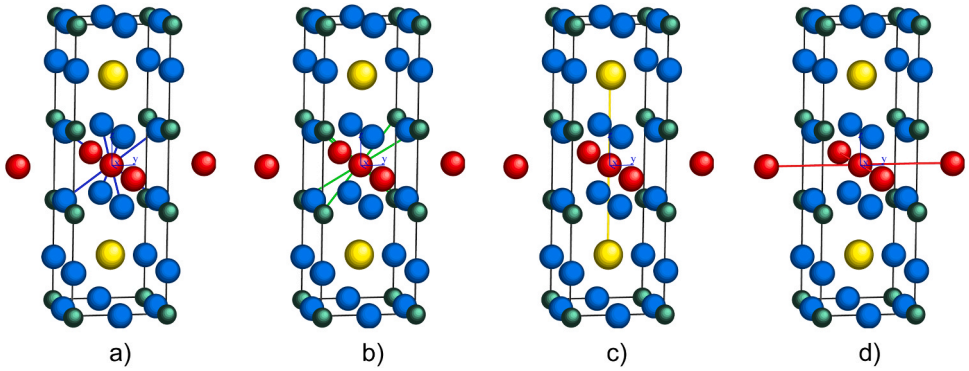

Fig. 6. Scheme of the unit cell: red spheres are Y/Gd atoms, oxygen atoms are blue, copper are green and barium atoms are yellow. The central Y/Gd atom has been connected to the first neighbours taken into consideration in the model: a) the first oxygen shell, b) the copper first neighbours, c) the two closest barium atoms, d) the next Y/Gd atoms.

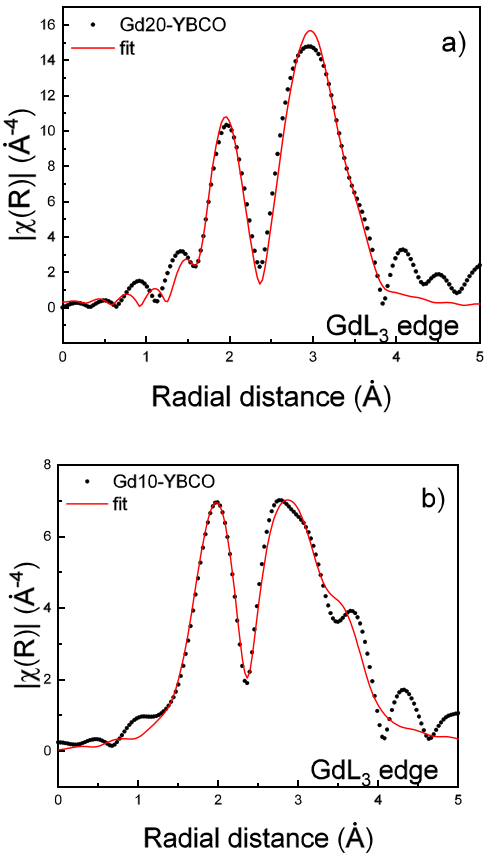

Fig. 7. a) GdL_3 edge. Black dotted line: FFT modulus of the Gd20% doped-YBCO EXAFS signal. Red continuous line: model fit; R-factor = 0.0254. b) GdL_3 edge. Black dotted line: FFT modulus of the Gd10% doped-YBCO EXAFS signal. Red continuous line: model fit; R-factor = 0.0096. The Fourier Transformed EXAFS data were fitted in the R interval 1.3–4.0 Å.

secondary phases were not detected, thus are below the EXAFS detection limit (about 5% within the bulk). However, XRD spectra demonstrate that binary oxides, such as $(Y,Gd)_2Cu_2O_5$, were actually formed. They can be mainly identified as the particulates observed by SEM analyses on the film surface whose density increases with Gd content. Since EXAFS technique is recognized to be less sensitive to the phases present on the surface, we can conclude that most of the Gd-related secondary phases are segregated at the surface. From EXAFS, we obtain the key information about the incorporation of Gd on the Y site of the YBCO lattice. This result demonstrates that Y/Gd substitutions can be promoted in YBCO systems when Gd atoms are added in excess with respect to Y. EXAFS results ultimately encourage further studies aimed at the full assessment of the potentiality of the adopted synthesis approach for the optimization of YBCO film properties.

CRediT authorship contribution statement

P. Reale: Investigation, Formal analysis, Visualization, Writing - Review & Editing. **V. Pinto**: Resources, Investigation, Writing - Review & Editing. **P. Cayado**: Resources, Writing - Review & Editing. **G. Celentano**: Conceptualization, Writing - Review & Editing, Funding acquisition. **A. Angrisani Armenio**: Investigation. **A. Rufoloni**: Investigation. **A. Santoni**: Methodology, Investigation, Formal analysis, Visualization, Writing - Original Draft, Funding acquisition. **F. D'Acapito**: Methodology, Investigation, Formal analysis, Writing - Review & Editing.

Declaration of Competing Interest

The authors declare that they have no known competing financial interests or personal relationships that could have appeared to influence the work reported in this paper.

Data availability

Data will be made available on request.

Acknowledgements

This work has been carried out within the framework of the EUROfusion Consortium and has received funding from the Euratom programme 2014–2018 and 2019–2020 under grant agreement N° 633053. The views and opinions expressed herein do not necessarily reflect those of the European Commission.

ESRF and CERIC are acknowledged for providing beamtime on their respective user access programs (experiment MA-5251 and experiment A08–1–1097). LISA is a project (N. **DFM**.AD006.072) financed by Consiglio Nazionale delle Ricerche, Italy.

The funders had no role in the design of the study; in the collection, analysis or interpretation of data; in the writing of the manuscript or in the decision to publish the results.

References

[1] J.G. Bednorz, K.A. Müller, Possible High T c Superconductivity in the Ba - La- Cu- 0 System, Z. Phys. B. 64 (1986) 189–193.
[2] M.K. Wu, J.R. Ashburn, C.J. Torng, P.H. Hor, R.L. Meng, L. Gao, Z.J. Huang, Y. Q. Wang, C.W. Chu, Superconductivity at 93K in a new mixed-phase Y-Ba-Cu-O compound system at ambient pressure, Phys. Rev. Lett. 58 (1987) 908–910.
[3] D. Larbalestier, A. Gurevich, D.M. Feldmann, A. Polyanskii, High-Tc superconducting materials for electric power applications, Nature 414 (2001) 368–377.
[4] X. Obradors, High critical current nanocomposite REBa 2Cu 3O 7(RE = rare earth) tapes: towards a new era of ultra-high field magnetism, Supercond. Sci. Technol. 31 (2018) 110501–110503, https://doi.org/10.1088/1361-6668/aae2ce.
[5] J.P.F. Feighan, A. Kursumovic, J.L. MacManus-Driscoll, Materials design for artificial pinning centres in superconductor PLD coated conductors, Supercond. Sci. Technol. 30 (2017) 123001, https://doi.org/10.1088/1361-6668/aa90d1.
[6] A.K. Jha, K. Matsumoto, Superconductive REBCO thin films and their nanocomposites: the role of rare-earth oxides in promoting sustainable energy, Front. Phys. 7 (2019) 799-21, https://doi.org/10.3389/fphy.2019.00082.
[7] J.L. MacManus-Driscoll, S.R. Foltyn, Q.X. Jia, H. Wang, A. Serquis, L. Civale, B. Maiorov, M.E. Hawley, M.P. Maley, D.E. Peterson, Strongly enhanced current densities in superconducting coated conductors of YBa2Cu3O7–x + BaZrO3, Nat. Mater. 3 (2004) 439–443, https://doi.org/10.1038/nmat1156.
[8] J.L. MacManus-Driscoll, S.R. Foltyn, B. Maiorov, Q.X. Jia, H. Wang, A. Serquis, L. Civale, Y. Lin, M.E. Hawley, M.P. Maley, D.E. Peterson, Rare earth ion size effects and enhanced critical current densities in Y2/3Sm1/3Ba2Cu3O7−x coated conductors, Appl. Phys. Lett. 86 (3) (2005) 032505, https://doi.org/10.1063/1.1851006.
[9] M. Miura, T. Kato, M. Yoshizumi, Y. Yamada, T. Izumi, T. Hirayama, Y. Shiohara, Rare earth substitution effects and magnetic field dependence of critical current in Y1- x REx Ba2 Cu3 Oy coated conductors with nanoparticles (RE=Sm, Gd), Appl. Phys. Express 2 (2009) 023002–023003, https://doi.org/10.1143/apex.2.023002.
[10] P. Cayado, M. Erbe, S. Kauffmann-Weiss, A. Jung, J. Hänisch, B. Holzapfel, Chemical solution deposition of Y 1−xGd xBa 2Cu 3O 7−δ–BaHfO 3nanocomposite films: combined influence of nanoparticles and rare-earth mixing on growth conditions and transport properties, RSC Adv. 8 (2018) 42398–42404, https://doi.org/10.1039/c8ra09188a.
[11] P. Cayado, L. Grünewald, M. Erbe, J. Hänisch, D. Gerthsen, B. Holzapfel, Critical current density improvement in CSD-grown high-entropy REBa 2 Cu 3 O 7−δ films, RSC Adv. 12 (2022) 28831–28842, https://doi.org/10.1039/d2ra03807b.
[12] T.J. Haugan, J.C. Tolliver, J.M. Evans, J.W. Kell, Crystal chemical substitutions of YBa2Cu3O7-d to enhance flux pinning, in: A.V. Narlikar (Ed.), Studies of High Temperature Superconductors, Nova Science Publishers, Inc, 2005, pp. 193–211.
[13] C.S. Li, L.H. Jin, Z.M. Yu, S.N. Zhang, Y.F. Lu, J.Q. Feng, Y. Wang, P.X. Zhang, Enhanced flux pinning in YGdBCO film grown by sol–gel approach, J. Sol. Gel Sci. Technol. 70 (2014) 67–71, https://doi.org/10.1007/s10971-014-3275-y.
[14] S. Xu, X.S. Wu, G.B. Ma, Z.H. Wang, J. Gao, Effects of Gd2O3 addition in YBa2Cu3O7−δ on the critical current density, J. Appl. Phys. 103 (2008) 07C714, https://doi.org/10.1063/1.2839619.
[15] V. Pinto, A. Vannozzi, A.A. Armenio, F. Rizzo, A. Masi, A. Santoni, A. Meledin, F. M. Ferrarese, S. Orlanducci, G. Celentano, Chemical solution deposition of YBCO films with Gd excess, Coatings 10 (2020) 860-17, https://doi.org/10.3390/coatings10090860.

[16] M. Erbe, P. Cayado, W. Freitag, K. Ackermann, M. Langer, A. Meledin, J. Hänisch, B. Holzapfel, Comparative study of CSD-grown REBCO films with different rare earth elements: processing windows and Tc, Supercond. Sci. Technol. 33 (2020) 094002–094011, https://doi.org/10.1088/1361-6668/ab9aa0.
[17] X. Obradors, T. Puig, Coated conductors for power applications: materials challenges, Supercond. Sci. Technol. (2014), https://doi.org/10.1088/0953-2048/27/10/103001.
[18] Z. Li, M. Coll, B. Mundet, N. Chamorro, F. Vallès, A. Palau, J. Gazquez, S. Ricart, T. Puig, X. Obradors, Control of nanostructure and pinning properties in solution deposited YBa2Cu3O7−x nanocomposites with preformed perovskite nanoparticles, Sci. Rep. 9 (2019) 5828, https://doi.org/10.1038/s41598-019-42291-x.
[19] P. Cayado, B. Mundet, H. Eloussifi, F. Vallés, M. Coll, S. Ricart, J. Gázquez, A. Palau, P. Roura, J. Farjas, T. Puig, X. Obradors, Epitaxial superconducting GdBa 2Cu 3O 7− δ/Gd 2O 3nanocomposite thin films from advanced low-fluorine solutions, Supercond. Sci. Technol. 30 (2017) 125010–125012, https://doi.org/10.1088/1361-6668/aa8ffe.
[20] X. Obradors, T. Puig, Z. Li, C. Pop, B. Mundet, N. Chamorro, F. Vallés, M. Coll, S. Ricart, B. Vallejo, F. Pino, A. Palau, J. Gázquez, J. Ros, A. Usoskin, Epitaxial YBa2Cu3O7−x nanocomposite films and coated conductors from BaMO3 (M = Zr, Hf) colloidal solutions, Supercond. Sci. Technol. 31 (2018) 044001, https://doi.org/10.1088/1361-6668/aaaad7.
[21] T. Puig, J. Gutierrez, X. Obradors, Impact of high growth rates on the microstructure and vortex pinning of high-temperature superconducting coated conductors, Nat. Rev. Phys. (2023) 1–17, https://doi.org/10.1038/s42254-023-00663-3.
[22] J. Díez-Sierra, P. López-Domínguez, H. Rijckaert, M. Rikel, J. Hänisch, M.Z. Khan, M. Falter, J. Bennewitz, H. Huhtinen, S. Schäfer, R. Müller, S.A. Schunk, P. Paturi, M. Bäcker, K.D. Buysser, I.V. Driessche, High critical current density and enhanced pinning in superconducting films of YBa2Cu3O7−δ nanocomposites with embedded BaZrO3, BaHfO3, BaTiO3, and SrZrO3 nanocrystals, ACS Appl. Nano Mater. 3 (2020) 5542–5553, https://doi.org/10.1021/acsanm.0c00814.
[23] J.L. MacManus-Driscoll, S.C. Wimbush, Processing and application of high-temperature superconducting coated conductors, Nat. Rev. Mater. 6 (2021) 587–604, https://doi.org/10.1038/s41578-021-00290-3.
[24] G. Celentano, F. Rizzo, A. Augieri, A. Mancini, V. Pinto, A. Rufoloni, A. Vannozzi, J. L. MacManus-Driscoll, J. Feighan, A. Kursumovic, A. Meledin, J. Mayer, G. V. Tendeloo, YBa2Cu3O7x films with Ba2Y(Nb,Ta)O6 nanoinclusions for high-field applications, Supercond. Sci. Technol. 33 (2020) 044010, https://doi.org/10.1088/1361-6668/ab6ee5.
[25] V. Pinto, R. Lamanna, A. Vannozzi, A.A. Armenio, G.D. Marzi, A. Augieri, L. Piperno, G. Sotgiu, G. Celentano, Solution refining for MOD-YBCO optimization: an NMR study, IEEE Trans. Appl. Supercond. 28 (2018) 7500505, https://doi.org/10.1109/tasc.2018.2800767.
[26] M. Erbe, J. Hänisch, T. Freudenberg, A. Kirchner, I. Mönch, S. Kaskel, L. Schultz, B. Holzapfel, Improved REBa2Cu3O7−x (RE = Y, Gd) structure and superconducting properties by addition of acetylacetone in TFA-MOD precursor solutions, J. Mater. Chem. A 2 (2014) 4932–4944, https://doi.org/10.1039/c3ta15243j.
[27] F. d'Acapito, G.O. Lepore, A. Puri, A. Laloni, F.L. Manna, E. Dettona, A.D. Luisa, A. Martin, The LISA beamline at ESRF, J. Synchrotron Radiat. 26 (2019) 551–558, https://doi.org/10.1107/s160057751801843x.
[28] B. Ravel, M. Newville, ATHENA, ARTEMIS, HEPHAESTUS: data analysis for X-ray absorption spectroscopy using IFEFFIT, J. Synchrotron Radiat. 12 (2005) 537–541, https://doi.org/10.1107/s0909049505012719.
[29] E.N. Maslen, V.A. Streltsov, N. Ishizawa, A synchrotron X-ray study of the electron density in C-type rare earth oxides, Acta Crystallogr Sect. B 52 (1996) 414–422, https://doi.org/10.1107/s0108768195013371.
[30] T. Lippmann, P. Blaha, N.H. Andersen, H.F. Poulsen, T. Wolf, J.R. Schneider, K.-H. Schwarz, Charge-density analysis of YBa2Cu3O6.98. Comparison of theoretical and experimental results, Acta Crystallogr Sect. Found. Crystallogr 59 (2003) 437–451, https://doi.org/10.1107/s0108767303012789.
[31] B.J. Kennedy, M. Avdeev, The Structure of C-type Gd2O3. A powder neutron diffraction study using enriched 160Gd, Aust. J. Chem. 64 (2011) 119–121, https://doi.org/10.1071/ch10310.
[32] Y.L. Page, T. Siegrist, S.A. Sunshine, L.F. Schneemeyer, D.W. Murphy, S. M. Zahurak, J.V. Waszczak, W.R. McKinnon, J.M. Tarascon, G.W. Hull, L. H. Greene, Structural properties of Ba2RCu3O7 high-Tc superconductors, Phys. Rev. B 36 (1987) 3617–3621, https://doi.org/10.1103/physrevb.36.3617.
[33] G. Kresse, J. Furthmüller, Efficient iterative schemes for ab initio total-energy calculations using a plane-wave basis set, Phys. Rev. B. 54 (1996) 11169–11186, https://doi.org/10.1103/physrevb.54.11169.
[34] G.I. Csonka, J.P. Perdew, A. Ruzsinszky, P.H.T. Philipsen, S. Lebègue, J. Paier, O. A. Vydrov, J.G. Ángyán, Assessing the performance of recent density functionals for bulk solids, Phys. Rev. B 79 (2009) 155107, https://doi.org/10.1103/physrevb.79.155107.
[35] J.-W. Lee, S.-M. Choi, J.-H. Song, J.-H. Lee, S.-H. Moon, S.-I. Yoo, Stability phase diagram of GdBa2Cu3O7- δ in low oxygen pressures, J. Alloy. Compd. 602 (2014) 78–86, https://doi.org/10.1016/j.jallcom.2014.02.170.
[36] P. Cayado, M. Erbe, S. Kauffmann-Weiss, C. Bühler, A. Jung, J. Hänisch, B. Holzapfel, Large critical current densities and pinning forces in CSD-grown superconducting GdBa 2Cu 3O 7− x-BaHfO 3nanocomposite films, Supercond. Sci. Technol. 30 (2017) 094007–094013, https://doi.org/10.1088/1361-6668/aa7e47.
[37] P. Cayado, H. Rijckaert, E. Bruneel, M. Erbe, J. Hänisch, I.V. Driessche, B. Holzapfel, Importance of the pyrolysis for microstructure and superconducting properties of CSD-grown GdBa2Cu3O7−x-HfO2 nanocomposite films by the ex-situ approach, Sci. Rep. 10 (2020) 19469, https://doi.org/10.1038/s41598-020-75587-4.